Accidental release in the bunkering of LNG: Phenomenological aspects and safety zone

Published Version:
Carboni M., Pio G., Mocellin P., Vianello C., Maschio G., Salzano E. (2022). Accidental release in the bunkering of LNG: Phenomenological aspects and safety zone. OCEAN ENGINEERING, 252, 1-9 [10.1016/j.oceaneng.2022.111163].

Availability:
This version is available at: https://hdl.handle.net/11585/897320 since: 2022-10-25

Published:
DOI: http://doi.org/10.1016/j.oceaneng.2022.111163

Accidental Release in the Bunkering of LNG: Phenomenological Aspects and Safety Zone

Mattia ***CARBONI***[1], *Gianmaria* ***PIO***[2], *Paolo* ***MOCELLIN***[1], *Chiara* ***VIANELLO***[1], *Giuseppe* ***MASCHIO***[1], *Ernesto* ***SALZANO***[2,*]

[1] Dipartimento di Ingegneria Industriale, Università degli Studi di Padova. Via Marzolo 9, 35131 Padova, Italia

[2] Dipartimento di Ingegneria Civile, Chimica, Ambientale e dei Materiali, Università degli studi di Bologna, Via Terracini 28, 40131 Bologna, Italia

*Author to whom correspondence should be addressed: ernesto.salzano@unibo.it

Abstract

The continuous increase in consciousness on properties and models characterizing cryogenic fuels has opened a new era for the supply of alternative sources of energy, especially in the naval sector. However, practical insights providing comprehensive indications for the development of safe and optimized procedures are still missing or lacking. In this perspective, a preliminary investigation on the commonly adopted procedure was integrated with a 3-dimensional representation of a typical port area in computational fluid dynamics (CFD) simulations implementing sub-models suitable for cryogenic conditions. At first, different scenarios were selected as representative for possible release conditions: Unloading Operation (UO), Shore to Ship (STS), and Truck to Ship (TTS) bunkering operations. This study indicates that TTS can be the most critical scenario because of the simultaneity of bunkering and disembarking procedures. The numerical analysis was devoted to the quantification of the safety distance in the case of the absence of an ignition source. The area where skin and eyes' frostbite are possible is assessed, as well, based on the combination of estimated temperature and local wind speed. The resulting safety distances were compared against estimations deriving by discrete and integral models without obstacles, demonstrating that neglect obstacles lead to non-conservative results. Indeed, a local increase in mixing effectiveness, limiting the flammable area within the channel between quayside and ship, was identified and characterized in this work. Besides, it was found that only under certain circumstances for TTS operations a flammable cloud can potentially reach passengers. Hence, the installation of barriers and mitigation systems (e.g., water curtains) is strongly recommended.

Keywords: Liquefied Natural Gas; Dispersion; Bunkering; Safety; Numerical Modelling.

Highlights:

- Evaluation of safety distances on downwind direction after an LNG release
- Integration of CFD analysis with simplified 3D ports
- Comparison of estimations deriving by integral and discrete models
- Assessment of flammable region, height, and volume
- Quantification of the area where frostbite is possible

1. Introduction

The use of liquefied natural gas (LNG) has been significantly promoted by economic, environmental, political, and logistic factors (Chen et al., 2017)(Osorio-Tejada et al., 2017), raising new concerns on safety aspects due to the cryogenic conditions and interactions with industrial operators working in the port areas (Fy et al., 2016)(Chang and Park, 2019)(Aneziris et al., 2020). As a way of example, frostbite is the freezing of skin and tissues due to the instantaneous contact with cold substances or surfaces and can be categorized as first degree (superficial, "frostnip"), second degree (full skin), third-degree (subcutaneous tissue), and fourth-degree (extensive tissue and bone). It occurs when the temperature of the skin or the tissues is lower than 2 °C (for the short duration exposure), thus resulting in the formation of intracellular ice crystals and microvascular occlusion (Weinzweig, 2010). Similarly, freeze burns refer to damages produced by the prolonged exposure time of the human body to cold atmosphere or surfaces. Few cases are reported in the literature for LNG frostbites, whereas other reports can be found for other cryogenic liquids (Kumar and Chirayil, 1999) (Uygur et al., 2009) (Sever et al., 2008).

In this sense, the realization of a quantitative risk assessment (QRA) is highly desirable. This analysis can be intended as a combination of probabilistic and phenomenological approaches. The former aims at the assessment of the probability of a given scenario, whereas the latter quantifies the consequences related to this event. In both cases, results can be affected by several parameters. As a way of example, an accidental release of LNG can result in a pool fire, flash fire, or atmospheric dispersion based on the presence of immediate or delayed ignition, as reported in the literature (Pio and Salzano, 2019). The selection of specific scenarios should be driven by the probabilistic approach (Paik, 2020). However, it usually considers local parameters (e.g., atmospheric conditions) and peculiarity of the analyzed plant, showing a case-specific nature. On the other hand, some generalizations can be done to identify critical aspects in the commonly adopted procedures. In this view, ISO 20519: 2017 (ISO 20519, 2017) and ISO/TS 18683: 2015 (Publication, 2015) standards indicate bunkering as the most critical operation, suggesting procedures for the definition of safety zones and allowed activities. Once the scenario is identified, several procedures can be used for the quantification of safety distances associated to floating facilities during bunkering operations (Park et al., 2020). Besides, safety distances can be significantly affected by wind speed, wind direction, ship geometry and loading conditions (Park et al., 2018), suggesting the realization of dedicated investigations aiming at their quantification.

Different modalities can be adopted for the loading procedures in the naval sector such as: 1) LNG Unloading Operation (UO); 2) LNG Shore to Ship (STS) or Port to Ship (PTS); 3) Truck to Ship (TTS); 4) Ship to Ship (StS). In the UO, an LNG gas tanker discharges its product to a coastal deposit using fixed loading arms with large diameters. The LNG can be re-distributed from the shore to other ships through StS operations employing lower quantities and smaller loading arms. Alternatively, an LNG truck can be connected to the receiving ship on the quayside (TTS). In this operation, flexible hoses are used and lower LNG volumes are transferred. When a fixed structure is not present, the LNG can be delivered to the receiving vessels by another ship, boat or barge (StS). Here, flexible hoses are usually employed. For the dispersion of vapour, results given by deterministic procedures or over-simplified models are often considered as unreliable. Indeed, the European Maritime Safety Agency (EMSA) (European Maritime Safety Agency, 2017) suggests the use of detailed numerical models based on the computational fluid dynamics (CFD) approach. On the other hand, consequence analyses are commonly performed utilizing more user-friendly and simplified tools, namely the model Unified Dispersion Model (UDM). The mentioned tools can both be used to assess the stand-off distance in terms of the maximum distances at which the flammable cloud reaches the lower flammability limit (LFL) (D_{LFL}), as suggested by the ISO 20519: 2017 (ISO 20519, 2017).

Despite the existing guidelines, several aspects involving the estimation of the safety zone are still unclear or arguable. Thus, several efforts have been made to define robust procedures based on the evaluation of phenomenological aspects (Jeong et al., 2020) (Jeong et al., 2018). The presence of obstacles suggests the implementation of a 3D representation of the layout analyzed. Some examples of the implementation of a simplified 3D layout for the evaluation of methane dispersion can be found in the current literature (Baalisampang et al., 2019) (Carboni et al., 2021b).

This work is devoted to the numerical characterization of the cloud dispersion and, thus, the boundaries of the safety zone resulting from the accidental release of pure methane. The assessment of the safety zones was addressed in typical bunkering and transfer operations, which were differentiated and characterized in terms of specific parameters. At this scope, different approaches were applied starting from the procedure outlined by the Society for Gas as a Marine Fuel (SGMF). In particular, a CFD software that calculates the dispersion of vapour was chosen to include the presence of obstacles in the analysis. In addition, simplified approaches were used to compare the obtained results.

2. Methodology

2.1 Source term

The continuous release through an orifice was assumed a reversible adiabatic expansion (i.e., isentropic expansion). Considering that it is very unlikely that the flow of a liquid could be choked, the pressure in the orifice was supposed to be atmospheric. The following equations describe the expansion to the conditions in the orifice from the initial state (i) in which the methane was supposed at saturated conditions. More specifically, Equation 1 expresses the mass releasing flowrate ($\dot{m}$) and Equation 2 and Equation 3, the enthalpy (H_0) and the volume (V_0) in the orifice:

$$\dot{m} = C_d \cdot A_0 \cdot \frac{1}{V_0}\sqrt{2 \cdot (H_i - H_0)} \quad (1)$$

$$H_0 = H(T_0, P_0, F_{L0}) \quad (2)$$

$$V_0 = V(T_0, P_0, F_{L0}) \quad (3)$$

where C_d stands for the discharge coefficient, A_0 for the area of the orifice, T_0, P_0, F_{L0} for the temperature, the pressure, and the liquid fraction of the methane in the orifice, respectively. For incompressible fluids, a value of 0.6 is used for the discharge coefficient, following the literature (Uijt and Ale, 2005). The LNG leak can occur in different positions along with the systems and, consequently, have different orientations (i.e., vertical upwards/downwards, or horizontal). In the case of a vertical downward release, it is supposed that a pool is formed on a substrate, typically made by concrete or water. The formation of a vapour layer was assumed from the resulting liquid pool. Presuming the absence of mitigations systems, the pool footprint was assumed circular with radius r(t), with a uniform thickness h(t), related by Equation 4. In the conservation of the mass (Equation 5), the pool increases due to $\dot{m}$, and reduces because of pool evaporation E_{vap} (Equation 6) and dissolution on water (E_{sol}) (in case of release on water). E_{vap} is defined in Equation 6 based on power involved in boiling Q_{boil}, calculated as the net contribute of different heat transfer mechanisms (Equation 7). Conduction (Q_{cond}) from the ground was modelled assuming a uniform semi-infinite medium on which the pool spreads (Shaw and Briscoe, 1978).

$$M_{pool}(t) = \pi \cdot r^2(t) \cdot h(t) \cdot \rho_L \quad (4)$$

$$\frac{dM_{pool}(t)}{dt} = \dot{m}(t) - E_{vap}(t) - E_{sol}(t) \quad (5)$$

$$E_{vap}(t) = \frac{\max(Q_{boil}, 0)}{\Delta H_V(T_{pool})} \quad (6)$$

$$Q_{boil} = Q_{cond} + Q_{conv} + Q_{rad} + Q_{sol} + Q_{spill} \quad (7)$$

where t is the time, $M_{pool}(t)$ is the pool mass, ρ_L the density of the liquid, ΔH_V the heat of vaporization calculated as a function of the pool temperature (T_{pool}). The theory based upon Dodge et al. (1983) (Dodge et al., 1983) was used to consider the thermal contribute due to the dissolution (Q_{sol}). The method of Reid and Smith (Reid and Smith, 1978) was applied for the calculation of Q_{cond}. The method of Fleischer (1980) (Fleischer, 1980) was employed to calculate the power related to convection from the air into the pool Q_{conv}. Regarding the radiative contribute Q_{rad}, it is considered that the pool may gain heat from solar radiation and longwave radiation which may also make a small contribution. Moreover, for the spill-related contribute Q_{spil}, it is considered the diverse thermal capacity between the condition at the spill and the ones in the pool. Please consider that the thermal contribute due to ice formation was neglected because of the size of the water basin, as suggested by experimental and theoretical analyses (Vesovic, 2007). For the sake of conservative results, the times maximizing the pool dimensions and the evaporation rate were considered.

2.2 Consequence analyses

Typical examples of a consequence modelling tool that employ the Unified Dispersion Model (UDM) is PHAST (Process Hazard Analysis Software Tool) by DNV-GL (DNV, 2021). The main advantages of this software stand in an extensive validation (Witlox et al., 2012) and a user-friendly interface. Nevertheless, these models cannot account for complex terrain geometries and spatial obstacles in the model domain (Gerbec et al., 2021). On the other hand, Fire Dynamics Simulator represents an open-source code for CFD analyses, validated for the characterization of the safety of cryogenic systems (McGrattan et al., 2017) (McGrattan et al., 2019b). FDS solves numerically a form of the Navier-Stokes equations appropriate for low-speed thermally-driven flow. The formulation of the equations and the numerical algorithm are contained in the FDS Technical Reference Guide (McGrattan et al., 2017). In addition, some verified and validated models are discussed in the Verification (McGrattan et al., 2013) and Validation (McGrattan et al., 2019b) guides. Besides, it can be integrated with specific sub-models devoted to accurate estimations of peculiar phenomena occurring at the investigated conditions (Carboni et al., 2021a) (Pio et al., 2019). For the LNG case, numerical estimations have been compared with large-scale experimental campaigns, i.e., Burro, Coyote, Falcon, Maplin Sands (McGrattan et al., 2019b), as reviewed by Luketa-Hanlin (Luketa-Hanlin, 2006).

2.3 Boundary Conditions

Three different scenarios involving an LNG transfer operation were investigated: 1) LNG Unloading Operation (UO); 2) LNG Shore to Ship (STS); 3) Truck to Ship (TTS) bunkering operations. In this perspective, different ships and transfer conditions were considered (Table 1). More specifically, simplified geometries based on the overall dimensions preventing the expansion of the flammable cloud were assumed as representative for the analysed ships.

Table 1. Ships involved in the present study and corresponding transfer conditions. The main characteristics should be intended as simplified overall geometrical features and with the aim of a generic example.

	Unloading Operation (UO)	**Shore to Ship (STS)**	**Truck to Ship (TTS)**
Name	JS INEOS INTREPID	-	HYPATIA DE ALEJANDRIA
IMO	9685449	-	9498755
Vessel type	LNG tanker	LNG tanker	LNG ferry
Length overall [m]	180.0	86.0	186.0*
Height overall [m]	9.0	6.0 and 11.0	17.0
Breadth overall [m]	26.6	26.7	25.0
Manifold to bow distance [m]	96.4	49.6	158
Inventory [m^3]	27500	32000	40
Transfer system	Loading arm	Loading arm	Flexible hose
Transfer system diameter [inch]	12	6	2
Transfer pressure [barg]	7.55	5.55	12.00
Pool dimensions (x-direction, y-direction) [m]	4.0 x 1.6	2.0 x 1.6	2.0 x 1.6
$\boldsymbol{E_{vap}}$ **[kg s^{-1}m^{-2}]**	0.10	0.08	0.08

*Length on the water line equal to 172m. The last 14m of the stern was considered 0.5m above the water.

Regardless of the considered operations, the ship to quayside distance and the quayside height were set equal to typical values of 1.6 m (d_{q-s}) and (h_q) 2.0 m, respectively. Moreover, for the TTS case, the truck-ship distance ($L_{f.h.}$) was posed equal to15 m. The total volume transferred was estimated based on the analysed scenario, the type of the transfer system (i.e., flexible hoses or loading arms), the dimension of the transfer system, and the transfer pressure. The initial event was defined following the procedure suggested by the Society for Gas as a Marine Fuel (SGMF) (Bond et al., 2018), defining the worst-case scenario described in the deterministic approach of ISO 20519: 2017 (ISO 20519, 2017) as non-credible. Hence, the latter was neglected in consequence analyses performed in this work. Besides, a series of hole sizes depending on the size and the material of the loading arm (i.e., flexible or hard) is investigated. Then, the source model reported in Equation 1 was implemented to estimate the mass releasing flowrate ($\dot{m}$) for each scenario assuming pure methane, as commonly made in a numerical investigation (Pio and Salzano, 2018). Indeed, the presence of heavier hydrocarbons (e.g., ethane and propane) leads to smaller and less-lasting flammable clouds because of the compensation between decreased volatility and lower flammability limits (Eberwein et al., 2020). Hence, in the absence of an ignition source, pure methane can be considered as a representative of LNG.

Regarding the atmospheric conditions, an ambient temperature equal to 25 °C and the atmospheric Pasquill classes D (neutral), associated with a wind velocity equal to 5 m s^{-1}, and a relative humidity equal to 40% were implemented as per the case of dry and sunny conditions. On the other hand, the atmospheric Pasquill class F (very stable), associated with a wind of 2 m s^{-1}, and a relative humidity equal to 70 %, were implemented for the case of wet and foggy climatic conditions. In this view, eight scenarios for each operation (i.e., UO, STS, and TTS) were distinguished (Table 2).

Table 2. Main characteristics of the scenarios analyzed (UO, STS and TTS) in the 8 set of conditions.

Scenario	**1**	**2**	**3**	**4**	**5**	**6**	**7**	**8**
Wind [m s^{-1}]	5	2	5	2	5	2	5	2
Pasquill	D	F	D	F	D	F	D	F
Surface	Concrete	Concrete	Concrete	Concrete	Water	Water	Concrete	Concrete
Direction	Horizontal	Horizontal	Downward	Downward	Downward	Downward	Upward	Upward

The dispersion results were expressed in terms of downwind distance to LFL (4.4% v/v) and 0.5 LFL (D_{LFL} and $D_{0.5\ LFL}$) and maximum height at the LFL and 0.5 LFL (H_{LFL} and $H_{0.5\ LFL}$). Furthermore, the resulting total volumes of the vapour cloud at LFL and 0.5 LFL (V_{LFL} and $V_{0.5\ LFL}$) were derived. At this aim, where the loading arm is employed (i.e., UO and STS), the volumes can be calculated considering a circular base area with a diameter equal to D_{LFL} and $D_{0.5\ LFL}$ respectively and a height equal to H_{LFL} and $H_{0.5\ LFL}$. On the other hand, for the TTS bunkering, it is necessary to take into consideration the flexible hose length ($L_{f.h.}$) and that part of the safety zone boundaries is always defined by the scenarios involving water as substrate (Equation 8):

$$V_{LFL,i} = \left[\left(\frac{\pi D_{LFL,i}^2}{2}\right) + (2D_{LFL,i} \cdot L_{f.h.})\right] \cdot H_{LFL,i} + \left(\frac{\pi D_{LFL,water}^2}{2}\right) \cdot H_{LFL,water} \text{ with } i \neq 5,6 \quad (8)$$

where $D_{LFL,\ water}$ and $H_{LFL,\ water}$ are the distances calculated for TESTs 5 and TESTs 6.

CFD analyses were performed posing particular attention to the release on water. This specific situation may largely affect D_{LFL} and H_{LFL}, since high evaporation rate values and significant effects of obstacles and degree of congestion are expected. Numerical results were reported at the time maximizing the stand-off distances unless otherwise noted.

The LNG pool was supposed to be formed between the ship and the quayside in correspondence with the ship manifold. The centre of the pool was considered as the axis origin. The size of the pool on y-direction was equalized to d_{q-s} and, the size on x-direction was derived by Equation 4. The evaporation rate was derived by Equation 5. A given value for the heat flux from the substrate was chosen following data reported for the Coyote3 test (313.5 W m^{-2}) (McGrattan et al., 2019a)(McGrattan et al., 2019b). In the case of the TTS scenario, being the ship involved an LNG ferry, the bunkering was considered as simultaneous to the disembarkation/embarkation of the passengers, as provided for in the EMSA guidelines (European Maritime Safety Agency, 2017), and thus with the unloading ramp lying on the quayside. The size of the numerical grid was kept constant (i.e., with cell sizes of 0.125 x 0.125 x 0.125 m). Please note that, when large areas are taken into consideration, the grid cannot be fine enough to capture the mixing processes at all relevant scales. To this aim, a subgrid-scale model is employed (Smagorinsky, 1963). The large-eddy simulation (LES) equations are derived by applying a low-pass filter, parameterized by a width, to the transport equations for mass, momentum, and energy. In FDS, the filter width is equivalent to the local cell size and is a key parameter in the models accounting for the turbulent viscosity and the reaction time scale. Additional details can be found in the mathematical model reported in the Technical Reference Guide (McGrattan et al., 2017).

For the sake of clarity, images representing the three situations are reported (Figure 1)

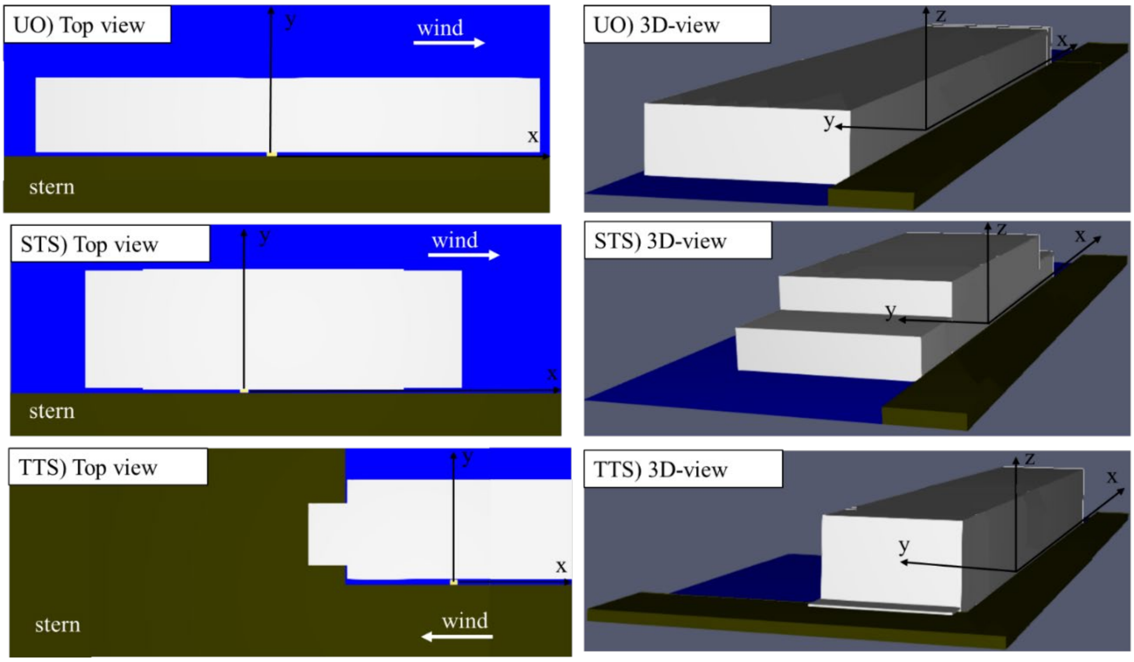

Figure 1. Top and lateral view of the simplified layouts adopted in this work, representative of a typical port facility during LNG transfer operations.

Furthermore, the differences between the safety distances calculated using the LFL and the half LFL as threshold values in the case of water substrate was quantified through Equation 9.

$$\frac{x_{0.5LFL,j}}{x_{LFL,j}} = \left(\sum_{k=5,6} \frac{x_{0.5LFL_{k,j}}}{x_{LFL_{k,j}}}\right) \cdot \frac{1}{2} \qquad (9)$$

where x is the generic safety parameter (i.e., D, H, and W), j the transfer operation (i.e., UO and STS), and k the k-th set of conditions involving water as substrate (i.e., 5 and 6).

For the sake of comparison, the same FDS simulations were conducted without considering the presence of obstacles and thus following the same geometrical approach of PHAST. In this way, it was possible to compare the three methods better and quantify the importance of considering the obstacles. At this aim, the results produced by the three different approaches (i.e., PHAST and FDS neglecting and considering the presence of obstacles) were compared introducing the following quantities:

$$x_{FDS}^{PHAST} = \frac{x_{PHAST}}{x_{FDS\ no\ obstalces}} \qquad (10)$$

$$x_{FDS\,obst.}^{PHAST} = \frac{x_{PHAST}}{x_{FDS\,obstalces}} \quad (11)$$

$$x_{FDS}^{FDS\,obst.} = \frac{x_{FDS\,obstacles}}{x_{FDS\,no\,obstalces}} \quad (12)$$

To estimate the area potentially involved in skin and eyes' frostbite, the wind chill temperature ($T_{w.c.}$). was calculated. Indeed, this parameter account for the perceived temperature on human skin based on the rate of heat loss from exposed skin, i.e., combining the effect of wind and cold. The National Weather Service provides a correlation starting from the measured temperature (T) and the wind velocity (V_w) (NWS, 2021) (Equation 11):

$$T_{w.c.} = 35.74 + 0.6215 \cdot (32 \cdot T - 32) \cdot \frac{5}{9} - 35.75 \cdot V_w{}^{0.16} + 0.4275 \cdot (32 \cdot T - 32) \cdot \frac{5}{9} \cdot V_w{}^{0.16} \quad (10)$$

$T_{w.c.}$ was used to define the boundaries of an area where human-being can suffer from frostbite. More specifically the wind chill chart commonly adopted in the literature (Morris, 2007)(Kiss, 2012) was employed under the assumption of an exposure time of 5, 10, and 30 minutes.

Results and discussion

FDS results considering the presence of obstacles are presented at first. More specifically, results are introduced in the form of images in the following figures considering different views (i.e., top, lateral, and 3D). Then, they are presented and compared in terms of safety distances.

The unloading operation considering the water as substrate and 5D as atmospheric conditions (i.e., UO) is considered the base case. Figure 2 reports the methane distribution for the UO5 scenario, whereas results related to the other cases are reported in the supplementary material.

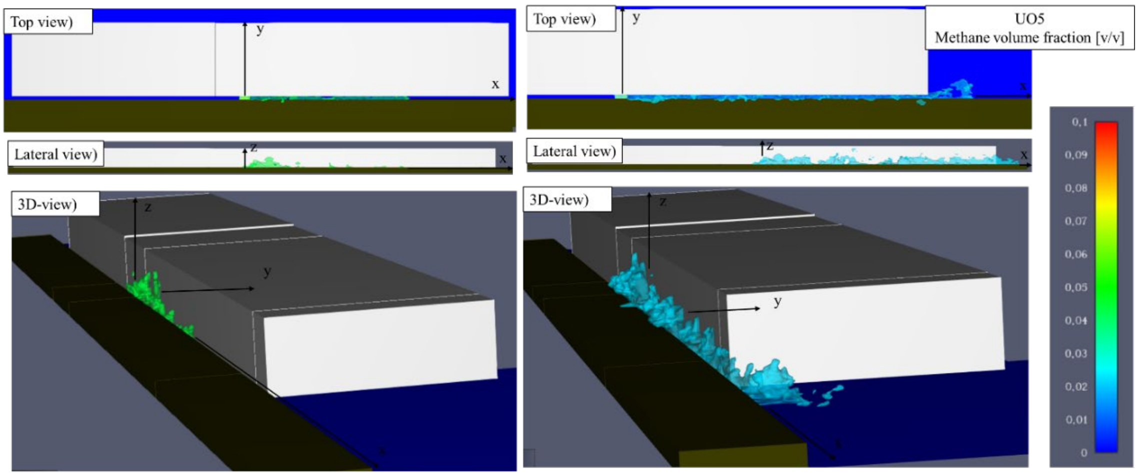

Figure 2. FDS results expressed in terms of methane volume fraction isosurfaces [v/v] viewed from different points in the UO5 scenario. The light blue colour cloud is the isosurface at 0.5LFL, while the green one is at LFL.

If the flammable cloud is limited to the area where a molar fraction higher than LFL can be found in the UO5 scenario, it is completely included within the area delimited by ship and quayside. On the other hand, the widespread assumption suggesting the use of half LFL as a threshold value to delimit the flammable area leads to a stand-off distance exceeding the ship end by 19 m on the downwind direction (positive x-direction) and 4.4 m in the perpendicular one (positive y-direction). In the 2F conditions (i.e., scenario UO6, Figure S1), a similar trend can be identified. The main difference between the two atmospheric conditions can be retrieved in the time history of flammable cloud areas. Indeed, initially, the cloud is colder, consequently heavier than air, and therefore less influenced by the wind. For this reason, the cloud spreads on both sides of the pool. In the second phase, i.e., when the temperature rises, the cloud becomes lighter than air favouring the dispersion in the downwind direction. The heat exchange is more effective when the wind velocity is higher, thus the spreading phase is less lasting when a 5 m s^{-1} condition is considered. A dedicated analysis investigating these aspects will follow in this study. In both scenarios, the cloud develops its height preferentially along with the ship's walls rather than the quayside. Regarding the negative y-direction, the flammable cloud succeeds in overcoming the quayside. More specifically, it expands for 1.0 m and 3.3 m in the UO5 and UO6 scenarios, respectively. In both STS5 and STS6, the flammable cloud does not exceed the overall ship dimensions (Figure S2 and Figure S3). Regarding the quayside, it is overcome by the cloud only at t_2. More specifically, it expands for 2.7 m and 2.4 m in the STS5 and STS6 scenarios, respectively.

Bearing in mind the shape of the resulting flammable clouds when FDS is applied considering the 3-D layout, the equation necessary to calculate the safety volume is:

$$V_{LFL,i} = 2 \cdot \left[\left(D_{LFL,i} \cdot W_{LFL,i} \cdot H_{LFL,i}\right) - V_q\right] \tag{11}$$

where $W_{LFL,i}$ is the maximum width of the flammable cloud in the y-direction and V_q is the solid volume of the quayside that has to be subtracted. Factor 2 is introduced to take into consideration opposite wind directions. For the sake of the volume calculation, the maximum distances retrieved in each case were taken into consideration for the sake of conservative results.

The flammable clouds generated for the UO5 scenario are also evaluated in the absence of obstacles (Figure 3). The case with 2F conditions can be found in the supplementary material (Figure S4).

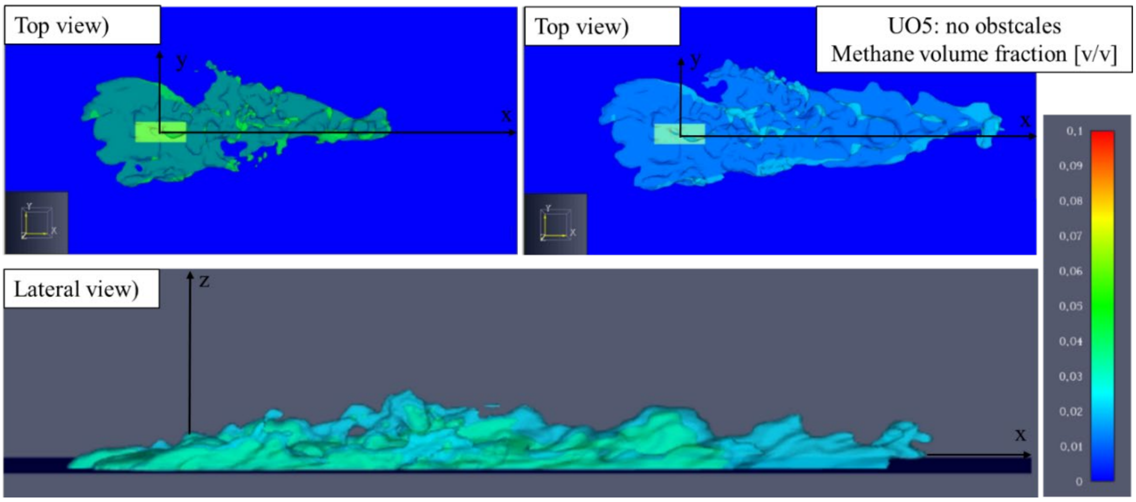

Figure 3. FDS results viewed from different points in the UO5 scenario when the presence of obstacles is neglected. The light blue colour cloud is the isosurface at 0.5LFL, while the green one is at LFL.

When the open field is considered, the resulting flammable cloud has similar dimensions in the x and y directions. After a preliminary phase in which the cloud develops in the wind direction, stabilization is reached. Lower values of downwind distance and flammable height are obtained concerning the case with obstacles due to the lack of confinement and the ship's wall effect. Similar results are obtained for the other scenarios. Starting from these considerations, safety distances are analyzed in the following Figure 4 in terms of downwind distance and height of the flammable cloud at LFL and 0.5 LFL. Furthermore, PHAST results are added, showing two distinguishable areas based on the threshold value considered (i.e., at LFL and 0.5 LFL). The first is characterized by a high and concentrated cloud, whereas the second shows a wider area. The scenarios that produce maximum D_{LFL} and H_{LFL} are the UO5 (40.5 m) and UO8 (5.5 m), respectively, identifying the UO as the operation that involves the largest safety area. On the other hand, the safety distances calculated in terms of the 0.5 LFL show a maximum $D_{0.5LFL}$ for UO4 and UO6 (i.e., 78 m and 70 m, respectively). These results confirm the on-water release as the one requiring particular attention. Conversely, the TTSs are intrinsically safer.

Regarding results obtained utilizing FDS, only the cases where obstacles are included provide larger areas than the ones obtained by PHAST at any corresponding conditions. Conversely, in the absence of obstacles (as it is for PHAST), FDS produces significantly narrower safety zones are obtained.

The UO scenarios produce larger areas with all the approaches considered, followed by STS. Regarding PHAST, TESTs 7 and 8 (vertical release) yield low values of safety volume except for the TTS scenario due to the different systems employed and thus different ways of the volume calculation. Additional details on the resulting safety volumes can be found in Figure S5. When the CFD is applied, safety volumes are dramatically reduced, and the lowest values are obtained when the obstacles are considered. Furthermore, 2F atmospheric conditions are not the most conservative in all the investigated scenarios.

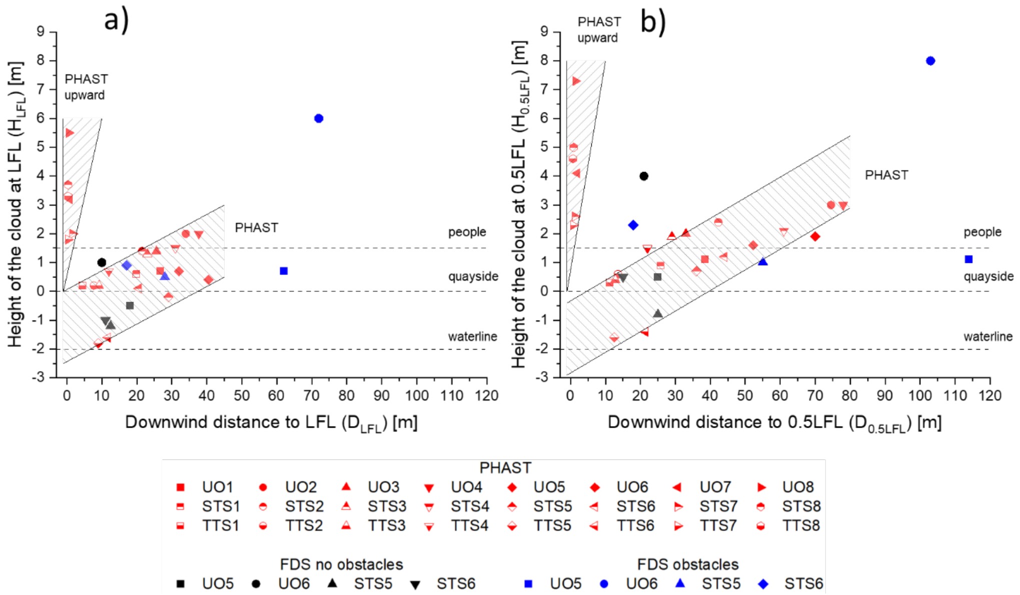

Figure 4. PHAST, FDS, and FDS with obstacles results expressed in terms of downwind distance and height of the flammable cloud at LFL (a) and 0.5 LFL (b).

The safety distances obtained by different methods are compared in Figure 5.

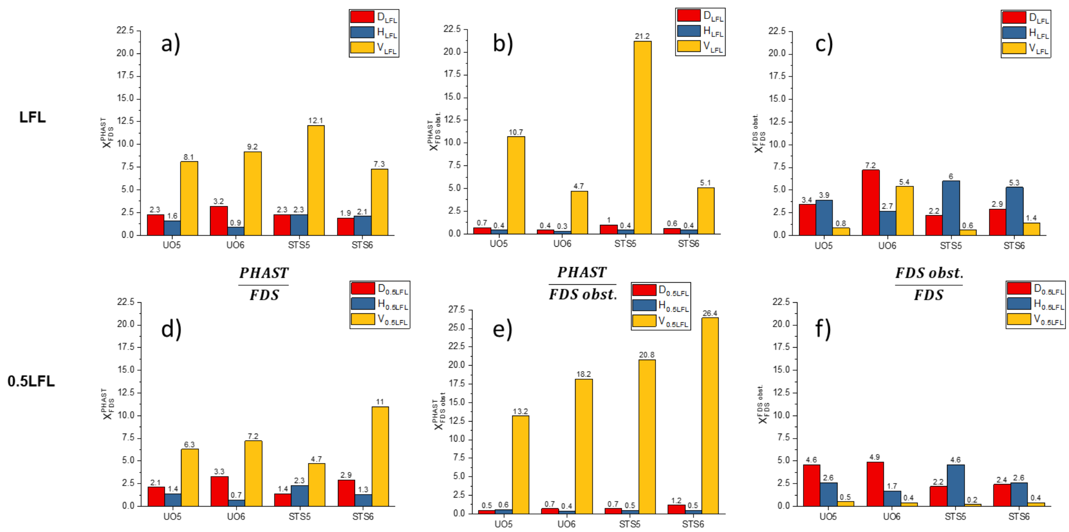

Figure 5. Safety distances at LFL (first row) and 0.5LFL (second row) produced by the three different approaches (i.e., PHAST and FDS neglecting and considering the presence of obstacles) applied to the scenarios considering water as substrate (i.e., 5 and 6).

PHAST produces almost double *H* and *D* than the case without obstacles evaluated by FDS. On the other hand, when the obstacles are introduced, estimated distances turn out to be higher than PHAST. Nevertheless, it is worth noting that PHAST provides larger volumes for any scenarios, meaning that larger areas reported once obstacles are considered in FDS simulations are mainly due to the congestion. A similar conclusion can be drawn when the two FDS approaches are compared. Consequently, the main positive aspect of the adoption of CFD models considering a real layout is the identification of the specific portion of volume involved in the cloud expansion. Indeed, depending on the wind direction, the presence of obstacles can narrow the flammable area in any direction perpendicular to the ship. In the proximity of the quayside, the safety zone should be extended for all the overall length of the ship, since in all the simulations, this zone is characterized by methane mole fractions larger than 0.5 LFL. On the other hand, these values are not reached beyond the ship, and thus the safety zone boundary in the y-direction can be identified by the ship wall. The presence of ship walls affects the velocity distribution, as reported in Figure 6 for the UO5 case at the time maximizing the downwind distances.

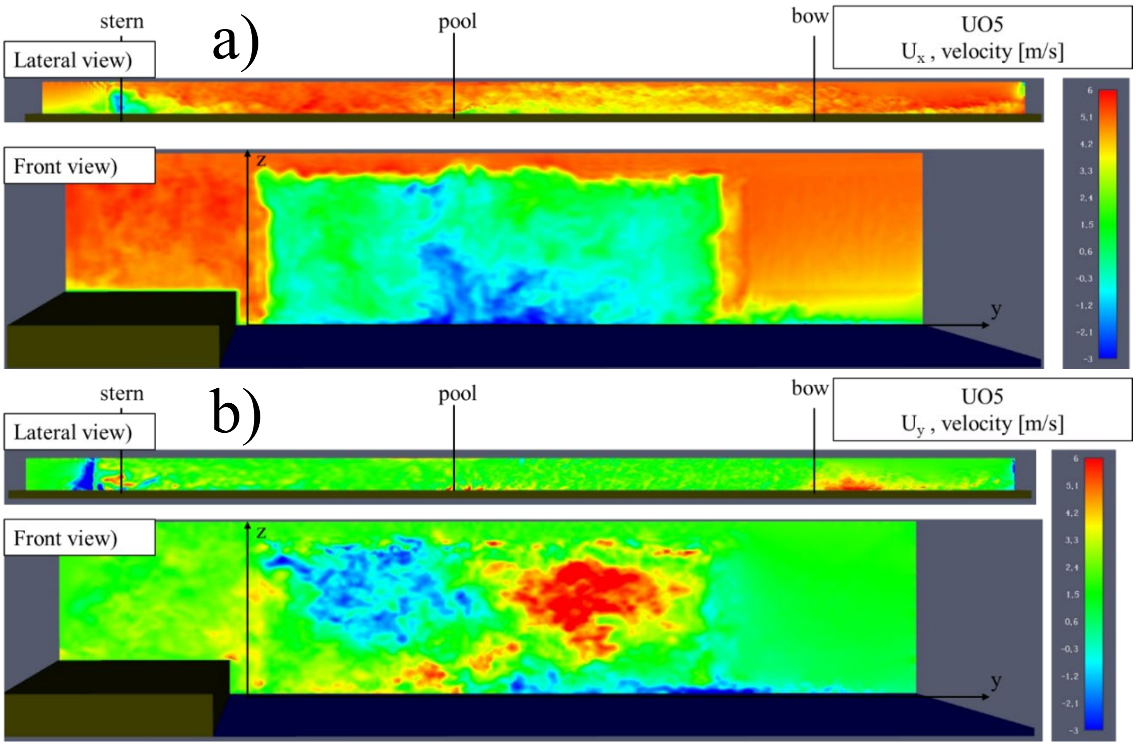

Figure 6. *Velocity in the x-direction (U_x) (a) and the y-direction (U_y) (b) of the UO5 scenario displayed from lateral and front. Please note that the Front view reports data obtained at 5 m from the bow in the downwind direction.*

Observing the lateral view, the regions where smaller rates can be found correspond to the fuel-rich pockets. This trend is attributable to fluid dynamics aspects since cold methane is denser than air in the proximity of the releasing point. On the other hand, the decreasing content of methane in the mixture, together with its increasing temperature, reduces this effect at a far-field distance. The combination of the U_x and U_y reported in Front views indicates the intensity of mixing phenomena induced by the expansion of the area available to the vapour. Indeed, Figure 7 confirms the presence of recirculating section since largely negative values can be observed for U_x, meaning that in a portion of the investigated section methane travels in the upwind direction. Similarly, Figure 8 shows largely positive U_y (up to 6 m s^{-1}) from the down-left corner to the top-right corner, whereas largely negative U_y (up to - 6 m s^{-1}) in the direction symmetric to the z-axis, although in this case, the component of the wind speed on the y-axis is null. Besides, the latter phenomena may extend the safety distances on the y-direction (W_{LFL}). This parameter should be defined taking into consideration the specific case since it is strictly dependent on h_q. In the case of a flexible hose as a transfer system, an on-land release is not negligible. Starting from these considerations, the safety zone should be extended accordingly, taking into consideration the release direction that produces more considerable distances (k-th set of conditions with $k \neq 5{,}6$). A simplified schematization is presented in Figure 7.

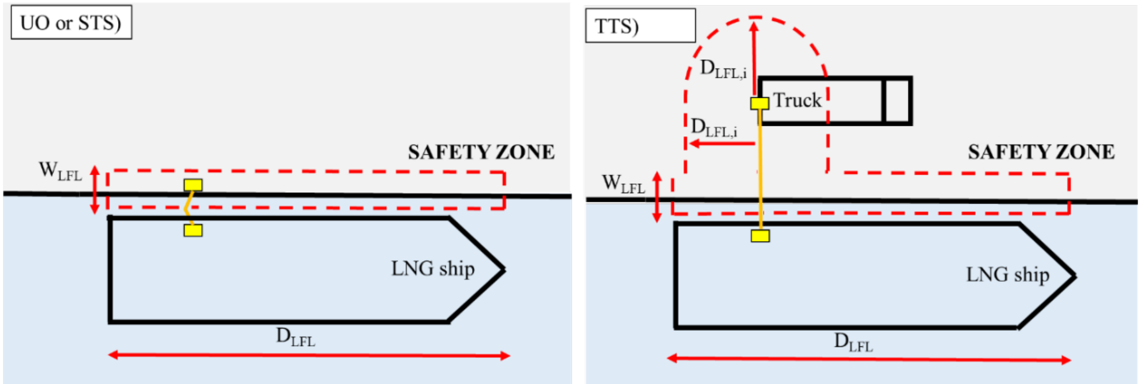

Figure 7. Safety zone application in case of use of a loading arm (left, UO, and STS) or flexible hose (right, TTS).

These results are conservative on the safe side if different wind directions and velocities are considered. Indeed, when the wind blows from the north-west or southwest at 5 m s^{-1} lower values of downwind distances are obtained (Figure S7). On the other hand, when the high wind velocity is considered (i.e, 10 m s^{-1}) similar downwind distances and lower height are obtained (Figure S8). According to the international standards (ISO 20519, 2017), the safety zone is assumed as a circular shape with a radius equal to D_{LFL}, when a loading arm is employed. Similarly, an elliptical-like shape is considered when a flexible hose is employed, having a semicircular extremity of D_{LFL} and centre-centre distance $L_{f.h.}$. A visual representation of these cases is reported in supplementary materials (Figure S6).

Regarding the differences in considering the beginning of the flammability concentration (i.e., 0.5 LFL) instead of lethality (i.e., LFL), it is possible to averagely consider the values reported in Table 7 expressed in terms of $\frac{D_{0.5\,LFL}}{D_{LFL}}$, $\frac{H_{0.5\,LFL}}{H_{LFL}}$ and $\frac{W_{0.5\,LFL}}{W_{LFL}}$.

Table 3. FDS results expressed in terms of $\frac{D_{0.5\,LFL}}{D_{LFL}}$, $\frac{H_{0.5\,LFL}}{H_{LFL}}$ and $\frac{W_{0.5\,LFL}}{W_{LFL}}$.

TEST	$\frac{D_{0.5\,LFL}}{D_{LFL}}$			$\frac{H_{0.5\,LFL}}{H_{LFL}}$			$\frac{W_{0.5\,LFL}}{W_{LFL}}$		
	PHAST	FDS	FDS Obst.	PHAST	FDS	FDS Obst.	PHAST	FDS	FDS Obst.
UO	1.7	1.7	1.6	1.5	1.8	1.2	2.2	1.0	1.6
STS	1.7	1.7	1.4	1.5	2.0	1.3	2.1	1.0	1.2

Quite similar ratios are obtained when the downwind distances are evaluated regardless of the method considered. On the other hand, when the heights of flammable clouds are examined large differences can be detected between the two CFD approaches. On y-direction (W), FDS (neglecting obstacles) produces similar clouds when the two thresholds are analyzed, whereas PHAST produces more than double areas. The introduction of obstacles in FDS results in an intermediate condition between the two alternative approaches discussed before.

As already reported in this work, one of the typical circumstances that are worth to be analysed is the disembarkation of an LNG ferry during a bunkering procedure. In this configuration, the quayside is also present in the proximity of the stern, where the disembarkation ramp is placed. In Figure 8, the flammable region in this configuration is presented for the 5D atmospheric class, whereas the case with 2F can be found in the supplementary material (Figure S9).

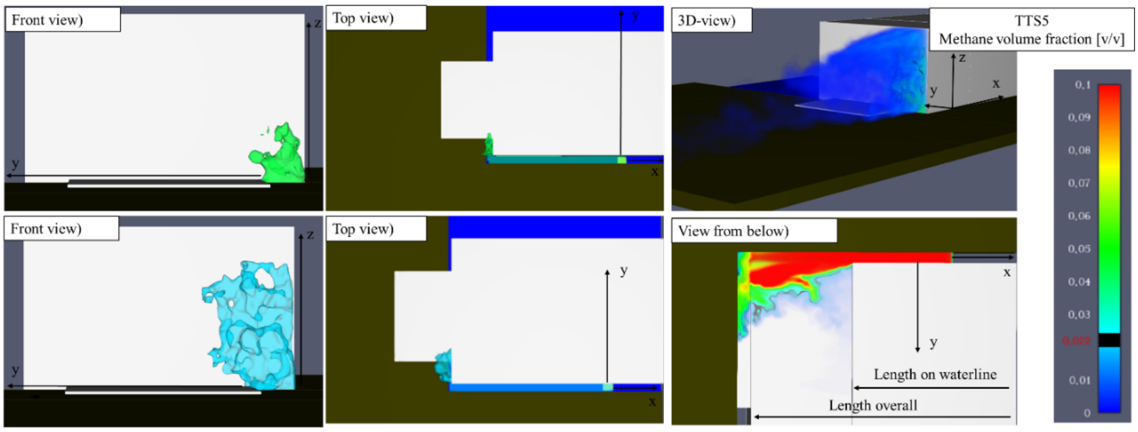

Figure 8. Methane distribution as obtained by FDS for the TTS5 scenario. Please note that the light blue colour cloud is the isosurface at 0.5 LFL, whereas the green one is at LFL.

As it is possible to note from Figure 10, the flammable cloud reaches the disembarkation ramp since the manifold is in proximity to the stern. Hence, part of the flammable cloud reaches passengers. Quite clearly, it is possible to affirm that this area is the most critical for the co-existence of an elevated grade of congestions and the possible presence of passengers and vehicles. The latter can also be intended as an additional source of ignition. For these reasons, specific barriers or mitigation systems (e.g., water curtain) should be considered. Based on the typical geometry of the investigated ship, a height of 0.5 m on the water level was implemented (view from below of Figure 10). This permits us to consider the expansion of the cloud in this area and observe that a high methane concentration in the air is methane (i.e., larger than 0.1 v/v). Furthermore, flammable areas are observed above the ramp (front view of the ship), contributing to increasing the concerns on this area. However, no significant expansion on the quayside is observed.

Considering the presented results, only the temperature distribution obtained for the TTS5 scenario is reported in this manuscript. Indeed, the TTS5 scenario represents the only case where a detailed analysis on possible frostbite is necessary, because of the coexistence of passengers without specific protective clothing and cold vapours in the proximity of the quayside. At this aim, the frostbite danger was assessed at different wind velocities (V_w) and exposure times. The resulting safety distances from the pool centre were reported in Table 4.

Table 4. Frostbite safety distances (m) as a function of wind velocity (ms^{-1}) and exposure time (min).

Wind velocity (V_w) [m s^{-1}]	**Frostbite safety distances [m]**		
	5 min	10 min	30 min
5	11	16	22
10	13	18	22
15	15	19	23
20	17	19	23
25	18	21	24

Based on the reported results it is possible to conclude that frostbite does not represent a significant issue from a safety perspective for LNG bunkering procedures, even in the case of simultaneous disembarking. Indeed, the related distances are included in the flame envelope considered for the assessment of safety distances for the flash fire scenario also in the case of large exposure time.

Conclusions

This article presents a numerical characterization of the safety aspects related to an accidental release of liquefied natural gas in port areas under a wide range of conditions, in absence of an ignition source. In particular, different layouts representative for ships, as well as alternative operations, potentially used for cryogenic fuels were analysed through the implementation of three-dimensional structures in computational fluid dynamics, integrated by sub-models suitable for cryogenic conditions. The obtained fuel distribution was used for the evaluation of the safety distance related to a flash fire, whereas the combination of temperature distribution and wind speed was used to individuate the area potentially involved by frostbite. Results deriving from integral and discrete approaches were compared in terms of safety distances, flammable volume, and size under the hypothesis commonly adopted for the characterization of flash fire. Although the introduction of obstacles leads to an increase in the flammable region, all of them were found to be limited to the proximity of the ships. This phenomenon was attributed to the increased effectiveness in fuel-air mixing, as testified by the velocity distribution reported in this work. Eventually, the possible presence of passengers within the flammable area deriving from an accidental release under the investigated conditions was detected only for the Truck to Ship bunkering operations, suggesting the installation of proper mitigation systems. Hence, the current study provides a robust and phenomenological-based background for the realization of safe infrastructures and procedures dealing with cryogenic fuels.

References

Aneziris, O., Koromila, I., Nivolianitou, Z., 2020. A systematic literature review on LNG safety at ports. Saf. Sci. 124, 104595. https://doi.org/10.1016/j.ssci.2019.104595

Baalisampang, T., Abbassi, R., Garaniya, V., Khan, F., Dadashzadeh, M., 2019. Accidental release of Liquefied Natural Gas in a processing facility: Effect of equipment congestion level on dispersion behaviour of the flammable vapour. J. Loss Prev. Process Ind. 61, 237–248. https://doi.org/10.1016/j.jlp.2019.07.001

Bond, S., Boon, C., Boreman, J., Dalkakis, D., de Souza, C., Eiermann, G., Eltringham, J., Haynes, D., Jaerschel, D., Johnson, M., LaRoche, M., Linsner, E., Peeters, R., Garrido, G.L., 2018. Gas as a marine fuel - Recommendation of Controlled Zones during LNG bunkering, Energy Policy. https://doi.org/10.1016/j.enpol.2015.08.027

Carboni, M., Pio, G., Mocellin, P., Vianello, C., Maschio, G., Salzano, E., 2021a. On the flash fire of stratified cloud of liquefied natural gas. J. Loss Prev. Process Ind. 75, 104680. https://doi.org/10.1016/j.jlp.2021.104680

Carboni, M., Pio, G., Vianello, C., Salzano, E., 2021b. Safety distances for the sour biogas in digestion plants. Process Saf. Environ. Prot. 147, 1–7. https://doi.org/10.1016/j.psep.2020.09.025

Chang, Y.T., Park, H., 2019. The impact of vessel speed reduction on port accidents. Accid. Anal. Prev. 123, 422–432. https://doi.org/10.1016/j.aap.2016.03.003

Chen, Z., Zhang, F., Xu, B., Zhang, Q., Liu, J., 2017. Influence of methane content on a LNG heavy-duty engine with high compression ratio. Energy 128, 329–336. https://doi.org/10.1016/j.energy.2017.04.039

DNV, 2021. Process Hazard Analysis Software Tool (PHAST) [WWW Document]. URL https://www.dnv.com/software/services/phast/index.html (accessed 5.1.21).

Dodge, F.T., Park, J.T., Buckingham, J.C., Maggott, R.J., 1983. Revision and experimental verification of the hazard assessment computer system models for spreading, movement, dissolution and dissipation of insoluble chemicals spilled onto water, US Coast Guard Report CG-D-35-83.

Eberwein, R., Rogge, A., Behrendt, F., Knaust, C., 2020. Dispersion modeling of LNG-Vapor on land – A CFD-Model evaluation study. J. Loss Prev. Process Ind. 65, 104116. https://doi.org/https://doi.org/10.1016/j.jlp.2020.104116

European Maritime Safety Agency, 2017. Guidance on LNG Bunkering to Port Authorities and Administration. 31 January 430.

Fleischer, F.T., 1980. SPILLS: An evaporation/air dispersion model for chemical spills on land, Shell Westhollow Research Center, Houston, Texas.

Fy, G., Wand, J., Yan, M., 2016. Anatomy of Tianjin Port Fire and Eplosion: Process and Caused. Process Saf. Prog. 35. https://doi.org/10.1002/prs

Gerbec, M., Vidmar, P., Pio, G., Salzano, E., 2021. A comparison of dispersion models for the LNG dispersion at port of Koper, Slovenia. Saf. Sci. 144, 105467. https://doi.org/10.1016/j.ssci.2021.105467

ISO 20519, 2017. ISO 20519 Ships and marine technology — Specification for bunkering of liquefied natural gas fuelled vessels Navires 2017.

Jeong, B., Lee, B.S., Zhou, P., Ha, S. man, 2018. Determination of safety exclusion zone for LNG bunkering at fuel-supplying point. Ocean Eng. 152, 113–129. https://doi.org/10.1016/j.oceaneng.2018.01.066

Jeong, B., Park, S., Ha, S., Lee, J. ung, 2020. Safety evaluation on LNG bunkering: To enhance practical establishment of safety zone. Ocean Eng. 216, 107804. https://doi.org/10.1016/j.oceaneng.2020.107804

Kiss, T.L., 2012. Critical Care for Frostbite. Crit. Care Nurs. Clin. North Am. 24, 581–591.

https://doi.org/https://doi.org/10.1016/j.ccell.2012.07.001

Kumar, P., Chirayil, P.T., 1999. Helium vapour injury: A case report. Burns 25, 265–268. https://doi.org/10.1016/S0305-4179(98)00163-6

Luketa-Hanlin, A., 2006. A review of large-scale LNG spills: Experiments and modeling. J. Hazard. Mater. https://doi.org/10.1016/j.jhazmat.2005.10.008

McGrattan, K., Hostikka, S., McDermott, R., Floyd, J., Vanella, M., 2019a. Fire Dynamics Simulator User's Guide. NIST Spec. Publ. 1019 Sixth Ed. 347. https://doi.org/10.6028

McGrattan, K., Hostikka, S., McDermott, R., Floyd, J., Weinschenk, C., Overhold, K., 2019b. Fire dynamics simulator (FDS) validation technical reference guide volume 3 : Validation. NIST Spec. Publ. 1018 3. https://doi.org/10.6028/NIST.SP.1018-1

McGrattan, K., Hostikka, S., McDermott, R., Floyd, J., Weinschenk, C., Overhold, K., 2013. Fire Dynamics Simulator, Technical Reference Guide, Volume 2: Verification.

McGrattan, K., Hostikka, S., McDermott, R., Floyd, J., Weinschenk, C., Overholt, K., 2017. Fire Dynamics Simulator Technical Reference Guide Volume 1: Mathematical Model. NIST Spec. Publ. 1018-1 1. https://doi.org/10.6028/NIST.SP.1018

Morris, S.E., 2007. Cold-induced injury: frostbite, in: Herndon, D.N.B.T.-T.B.C. (Third E. (Ed.), Cold-Induced Injury: Frostbite. W.B. Saunders, Edinburgh, pp. 530–535. https://doi.org/https://doi.org/10.1016/B978-1-4160-3274-8.50044-1

NWS, 2021. National Weather Service: The New Improved Wind Chill Index [WWW Document]. URL https://www.weather.gov/ffc/wci (accessed 7.1.21).

Osorio-Tejada, J.L., Llera-Sastresa, E., Scarpellini, S., 2017. Liquefied natural gas: Could it be a reliable option for road freight transport in the EU? Renew. Sustain. Energy Rev. 71, 785–795. https://doi.org/10.1016/j.rser.2016.12.104

Paik, J.K., 2020. Advanced Structural Safety Studies With Extreme Conditions and Accidents. Springer, Singapore.

Park, S., Jeong, B., Yoon, J.Y., Paik, J.K., 2018. A study on factors affecting the safety zone in ship-to-ship LNG bunkering. Ships Offshore Struct. 13, 312–321. https://doi.org/https://doi.org/10.1080/17445302.2018.1461055

Park, S.I., Kim, S.K., Paik FREng, J.K., 2020. Safety-zone layout design for a floating LNG-Fueled power plant in bunkering process. Ocean Eng. 196, 106774. https://doi.org/10.1016/j.oceaneng.2019.106774

Pio, G., Carboni, M., Iannaccone, T., Cozzani, V., Salzano, E., 2019. Numerical simulation of small-scale pool fires of LNG. J. Loss Prev. Process Ind. 61, 82–88. https://doi.org/10.1016/j.jlp.2019.06.002

Pio, G., Salzano, E., 2019. The effect of ultra-low temperature on the flammability limits of a methane/air/diluent mixtures. J. Hazard. Mater. 362, 224–229. https://doi.org/10.1016/j.jhazmat.2018.09.018

Pio, G., Salzano, E., 2018. Laminar Burning Velocity of Methane, Hydrogen, and Their Mixtures at Extremely Low-Temperature Conditions. Energy & Fuels 32, 8830–8836. https://doi.org/10.1021/acs.energyfuels.8b01796

Publication, B.S.I.S., 2015. ISO / TS 18683 : 2015 Standards Publication Guidelines for systems and installations for supply of LNG as fuel to ships.

Reid, R.C., Smith, K.A., 1978. Confined boiling rates of liquefied petroleum gas on water, EE-77-S-02-4548 MIT.

Sever, C., Ulkur, E., Uygur, F., Celikoz, B., 2008. Hand burn caused by Freon gas. Burns 34, 1210–1212. https://doi.org/10.1016/j.burns.2007.09.017

Shaw, P., Briscoe, F., 1978. Evaporation from spills of hazardous liquids on land and water, SRD report R100.

Smagorinsky, J., 1963. General Circulation Experiments with the Primitive Equations. The Basic Experiment. Mon. Weather Rev. 91. https://doi.org/10.1126/science.26.653.25

Uijt, H.P.A.M., Ale, B.J.M., 2005. Guideline for quantitative risk assessment 'Purple book'.

Uygur, F., Sever, C., Noyan, N., 2009. Frostbite burns caused by liquid oxygen. J. Burn Care Res. 30, 358–361. https://doi.org/10.1097/BCR.0b013e318198a769

Vesovic, V., 2007. The influence of ice formation on vaporization of LNG on water surfaces. J. Hazard. Mater. 140, 518–526. https://doi.org/10.1016/j.jhazmat.2006.10.039

Weinzweig, J., 2010. Plastic Surgery Secrets Plus, 2nd ed.

Witlox, H.W.M., Harper, M., Pitblado, R., 2012. Validation of phast dispersion model as required for USA LNG siting applications. 12th Top. Conf. Gas Util. 2012 - Top. Conf. 2012 AIChE Spring Meet. 8th Glob. Congr. Process Saf. 31, 263–275.